

# Chapter 4

## Analysis of Physical Cutting Mechanisms and Their Effects on the Tool Wear and Chip Formation Process When Machining Aeronautical Titanium Alloys: Ti-6Al-4V and Ti-55531

Mohammed Nouari and Hamid Makich

**Abstract** The current research deals with the analysis of physical cutting mechanisms involved during the machining process of titanium alloys: Ti-6Al-4V and Ti-55531. The objective is to understand the effect of all cutting parameters on the tool wear behavior and stability of the cutting process. The investigations have been focused on the mechanisms of chip formation and their interaction with tool wear. At the microstructure scale, the analysis confirms the intense deformation of the machined surface and shows a texture modification. As the cutting speed increases, cutting forces and temperature show different progressions depending on the considered microstructure Ti-6Al-4V or Ti-55531 alloy. Results show for both materials that the wear process is facilitated by the high cutting temperature and the generation of high stresses. The analysis at the chip-tool interface of friction and contact nature (sliding or sticking contact) shows that the machining Ti-55531 often exhibits an abrasion wear process on the tool surface, while the adhesion and diffusion modes followed by coating delamination process are the main wear modes when machining the usual Ti-6Al-4V alloy. Moreover, the proposed study describe the real effect on machining of the tool geometry, coating and lubrication. Finally, the investigations allow to identify some ways to improve the machinability of these alloys, particularly the Ti-55531 alloy.

---

M. Nouari (✉)

Laboratoire D'Énergétique et de Mécanique Théorique et Appliquée, LEMTA CNRS-UMR 7563, GIP-InSIC, 27 Rue D'Hellieule, 88100 St-Dié-Des-Vosges, France  
e-mail: mohammed.nouari@univ-lorraine.fr

M. Nouari

University of Lorraine/Mines Nancy, Mines Nancy, France

H. Makich

Laboratoire D'Énergétique et de Mécanique Théorique et Appliquée, LEMTA CNRS-UMR 7563, GIP-InSIC/Mines D'Albi, 27 Rue D'Hellieule, 88100 St-Dié-Des-Vosges, France

## 4.1 Introduction

Titanium alloys are widely used for applications requiring an excellent mechanical resistance and high strength at elevated temperature. This is the case of the Boeing 787 and A350 whose several structural parts are made in a new titanium alloy: the Ti-55531. This alloy has high mechanical characteristics that allow better performance on commercial aircraft, and a significant gain compared to the commonly used Ti-6Al-4V alloy. Beyond its interesting ratio density/mechanical properties, the Ti-55531 alloy provides significant benefits for the demanding environment of aeronautics. This comes from its ability to maintain mechanical properties at high temperature, the fatigue strength and its excellent corrosion resistance [1, 2]. Clément et al. [3, 4] have reported that the high-level properties of titanium alloys depend on several strengthening mechanisms such as grain size, solid solution atoms, and precipitation hardening, which all can be tuned during the various forming processing steps, leading to particular microstructures.

In manufacturing production, titanium alloys are classified as hard to cut materials. The main problems encountered when machining titanium alloy are the low material removal rate and the short tool life because of the excessive wear exhibited during the chip formation process. The first findings of machining Ti-55531 alloy are manifested by low cutting speeds. This causes high cycle times and reduced tool life, and then generates an increase in manufacturing costs.

Titanium is chemically reactive and, therefore, has a tendency to weld to the cutting tool during machining leading to chipping and premature tool failure [5–7]. In addition, its low thermal conductivity (about 15 W/m K vs. 270 W/m K for the steel CRS1018 at 700 °C) increases the temperature at the tool/workpiece interface, which adversely affects the tool life. Additionally, the high strength maintained at elevated temperature and low modulus of elasticity (50 % less than that of the steel) further impairs the machinability of these materials [6, 8, 9]. According to Ezugwu [10], the tool wear in machining of titanium alloys is due to high stresses and high temperatures found near to the cutting edge. The same conclusions were made by Subramanian [11].

From a microstructural point of view, elemental titanium presents an allotropic phase transformation at 880 °C between the body-centered cubic (bcc) and hexagonal-close-packed structures stable at high and low temperatures, respectively. The two phases of titanium alloys are known as  $\alpha$  phase and  $\beta$  phase respectively [12]. Combinations of working and heat treatment alter the microstructure and change the mechanical properties of the metal. The microstructure and properties can also be affected by adding other elements to titanium. Addition of other elements to pure titanium, i.e. alloying, can alter microstructure and properties as well. Depending on which phase is to be dominant in a particular alloy ( $\alpha$ ,  $\beta$  or  $\alpha + \beta$ ) an alloying element (or group of elements) may be added to pure titanium [3–5]. Thus, one way of classifying alloying elements is according to whether they are  $\alpha$  or  $\beta$  stabilizers. Alpha stabilizers are soluble in the  $\alpha$ -phase and many act as solid solution strengtheners while also increasing the temperature at which the

$\alpha$ -phase is stable. Alpha stabilizers include such elements as Al, Ga, Sn, Ge, and La. Beta stabilizing elements decrease the  $\beta$  transus (i.e., the temperature at which the material transforms to 100 %  $\beta$ -phase). As such, these elements increase the range over which the  $\beta$ -phase is stable. Beta stabilizers may be isomorphous or eutectoid. Isomorphous elements (such as V, Mo, Nb, Ta, and Re) are soluble in the  $\alpha$ -phase while eutectoid elements like (Cr, Fe, Mn, Cu, Ag, Au, Ni, and Co) create a eutectoid phase.

According to Fanning [13], Ti-55531 (TIMETAL 555) is a high-strength near- $\beta$  titanium alloy that was designed for improved productivity and excellent mechanical property combinations, including deep hardenability especially in aeronautical and aerospace industries. According to the same author and to Clément et al. in [3, 4], this recent alloy was designed based on the older Russian alloy VT22 to primarily fulfill high-strength forging applications. A lower-strength state with improved toughness and damage tolerance is under consideration for other parts of aircraft structure [14]. However, being of recent origin, there is a lack of information on machining of this alloy. This is despite the existence of information regarding thermomechanical processing of this family of alloys [15], and the abundance of information available regarding machining of titanium and some of its alloys (notably Ti-6Al-4V) [16]. In the machining field, it is well known that titanium and titanium alloys are hard-to-cut materials. This means that Ti-55531 will most likely present engineers with many technical problems to be solved in order to produce net shape components. Bouchnak recently proposed in [12] a study on the machinability of this material and assistance techniques to enhance the machining process. However, according to the literature in the field of machining, the state of the art does not present optimal solutions or does not give the real parameters that influence the cutting forces and tool wear (cutting conditions, tool geometry, and cutting material).

In order to increase productivity and tool-life in machining of titanium alloys, it is necessary to study the chip formation process and its effect on the physical cutting parameters and the material cutting performance. The objective of this study is to understand the poor machinability of titanium alloys especially the Ti-55531 one which exhibits extreme tool wear and unstable cutting forces.

## 4.2 Experimental Procedure

### 4.2.1 Workpiece Material

To analyse the machinability of the titanium alloys Ti-6Al-4V and Ti-55531, a parametric study has been conducted through several orthogonal cutting tests (cutting tests). Instrumented the Chip formation and tool wear processes have particularly been investigated in terms of cutting parameters such as cutting forces, friction coefficient and cutting temperature. Tests were carried out on a heavy-duty

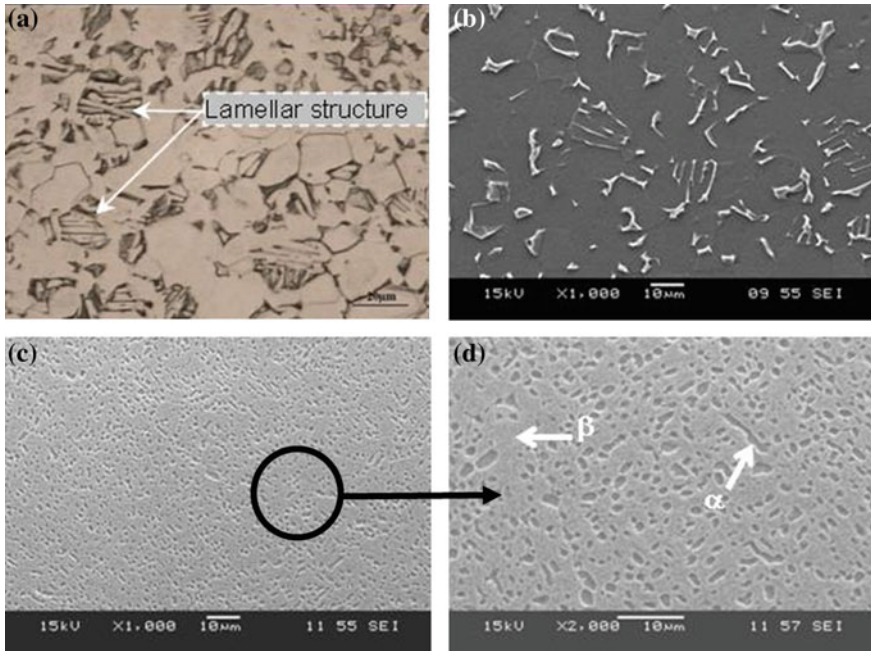


**Fig. 4.1** Microstructure of the workpiece material used in the current study before machining. **a** Optical micrograph of Ti-6Al-4V ( $\alpha + \beta$  alloy Ti-6Al-4V). **b** SEM micrograph of Ti-6Al-4V. **c** SEM micrograph of Ti-55531 ( $\beta$  alloy Ti-55531). **d** High magnification of SEM micrograph of Ti-55531

lathe machine with an 11 kW motor drive, which generates a maximum torque of 1,411 Nm. The spindle rotational speed ranges from 18 to 1800 rpm.

As mentioned above, two alloys were chosen for machining experiments. The first one is the alloy Ti-6Al-4V, considered as the reference of these tests. It is characterized with duplex structure  $\alpha/\alpha+\beta$ , and average grain size around 10  $\mu\text{m}$  (range from 5 to 20  $\mu\text{m}$ ). The second alloy studied here is the Ti-55531 with average grain size around 1  $\mu\text{m}$  (range from 0.5 to 5  $\mu\text{m}$ ).

Figure 4.1a–d depict the microstructure of each workpiece alloy before machining. The initial microstructure of the Ti-6Al-4V alloy, Fig. 4.1a, b, consists of single phase  $\alpha$  matrix. Inclusions of  $\beta$  grains can also be seen with average grain size of 10  $\mu\text{m}$  (range of 5–20  $\mu\text{m}$ ). Similarly, the initial microstructure of the  $\beta$  alloy Ti-55531 is shown in Fig. 4.1c, d. The microstructure consists of single phase  $\beta$  matrix with average size of  $\alpha$  grains of 5  $\mu\text{m}$  (range 1–5  $\mu\text{m}$ ).

In this work it has been found that the lamellar structure can be observed in  $\alpha + \beta$  colonies (transformed  $\beta$ ); particularly for the Ti-6Al-4V alloy. Figure 4.1a shows the localisation of the lamellar structure. This was previously confirmed by the work of Benedetti and Fontanari in [17].

**Table 4.1** Chemical composition of machined titanium

	Ti-6Al-4V	Ti-55531
Chemical element	(wt%)	(wt%)
Al	5.5	5
V	3.8	5
Fe	Max 0.8	0.3
Mo	0	5
Cr	0	3
Nb	0	0.5–1.5
Zr	0	0.5–1.5

**Table 4.2** Mechanical and thermal properties of Ti-6Al-4V and Ti-55531

	Ti-6Al-4V	Ti-55531
B transus ( $T_{\beta}$ ) (°C)	980	856
Density ( $\text{g/cm}^3$ )	4.43	4.65
Tensile elastic modulus (GPa)	110	112
Compressive elastic modulus (GPa)	–	113
Tensile strength (MPa)	931	1236
Yield strength (MPa)	862	1174
Elongation (%)	14	6
Thermal conductivity at 20 °C (W/m K)	7.3	6.2
Specific heat 20–100 °C (J/Kg K)	709	495

Table 4.1 presents a summary of the chemical composition of both alloys. According to Fanning [13], Nouari et al. [18] and Bouchnak [12], the physical properties of the Ti-6Al-4V and Ti-55531 alloys are summarized in Table 4.2.

To complete the characterization of studied titanium alloys, tests of Vickers hardness have been performed on different specimens under room temperature. The micro-hardness of the Ti-6Al-4V specimen was found to be about 317HV<sub>0.2</sub> and that measured for the Ti-55531 alloy to be about 379HV<sub>0.2</sub>. The Ti-55531 is therefore 20 % harder than Ti-6Al-4V. This result confirms the hard nature of the Ti-55531 microstructure, which will have a direct effect on its machinability, i.e. the level of cutting forces, tool wear, cutting temperature, etc.

## 4.2.2 Cutting Tools

### 4.2.2.1 Cutting Tool Material

In this study, inserts made of tungsten carbide (WC-Co) were used. The effect of the coating on the tool wear under extreme loading conditions was also investigated. To do that, a comparative study was performed between uncoated tool and coated one using a single layer of TiAlN coating with average thickness of 4  $\mu\text{m}$ .

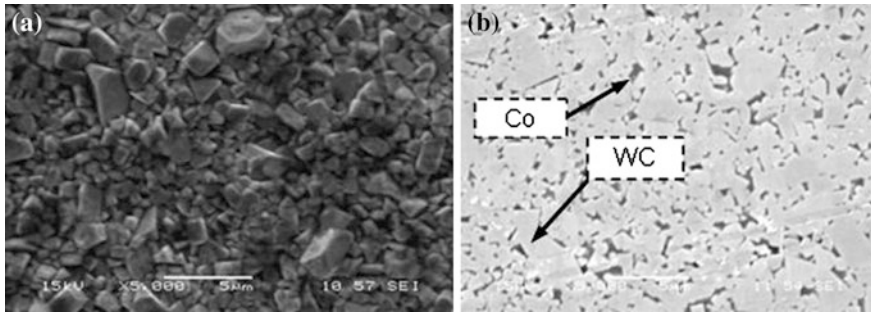


**Fig. 4.2** SEM micrograph of cemented carbide tool (WC-6 %Co). **a** Tool microstructure. **b** Co and Wc distribution at the tool surface

**Table 4.3** Mechanical and thermal properties of the cutting tool substrate [5, 6, 8]

Tool substrate	WC-6 %Co
Hardness 25 °C (HV <sub>10</sub> )	1,485
Hot hardness 800 °C (kg/mm <sup>2</sup> )	600
Density (g/cm <sup>3</sup> )	11.4
Thermal conductivity (W/mK)	45
Thermal expansion (10 <sup>-6</sup> /K)	6.1
Modulus of elasticity (GPa)	620
Traverse rupture (GPa)	2.2
Poisson coefficient $\nu$	0.26

The TiAlN coating has a strong chemical stability, a low thermal conductivity and an high oxidation wear resistance at 900 °C. The TiAlN coating increases the surface hardness to approximately 3400–3600 Hv and improves the resistance to abrasive wear. The thermal conductivity this coating is about 10 W/mK (at 20 °C). Devillez et al. [19] state that TiAlN coating imparts an excellent crater resistance. Additionally, Singh et al. [20] and Castanho et al. [21] show that the Al element incorporated in TiAlN coating forms the superficial layer Al<sub>2</sub>O<sub>3</sub> to improve the wear resistance and to enhance the chemical stability.

Therefore, the cutting tools used in these machining tests are made of tungsten carbide with cobalt binder, Grade H13A (WC-6 %Co, type K20). The tool microstructure is shown in Fig. 4.2a. Average and maximum sizes of the WC grains are respectively 1–5 μm. The average percentage of cobalt is about 6 %, the analysis under a scanning electron microscope (SEM) revealed that the Co binder is uniformly distributed in the tool surface, Fig. 4.2b. Table 4.3 presents a summary of the mechanical and thermal properties of cutting tools.

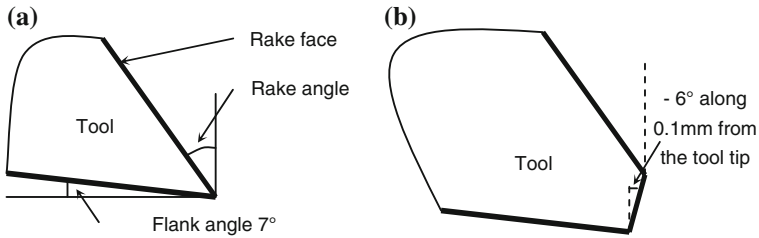


**Fig. 4.3** Presentation of the tool geometries used in machining tests. **a** Tool A, Rake angle constant along the rake face. **b** Tool B, two different rake angles along the cutting edge

#### 4.2.2.2 Cutting Tool Geometries

Concerning the tool geometry, a special designed tool (with two different geometries) has been considered in these experiments. Figure 4.3 shows the two geometries used in the study. The first geometry is more conventional without a particular treatment on the cutting edge, designated by geometry “A” (Fig. 4.3a). The second geometry is characterized by an additional angle of the cutting edge, designated by geometry “B” (Fig. 4.3b).

Tools for orthogonal cutting (width 4.45 mm) have one cutting edge and the flank angle is about 7°. Also, the tool “A” has a rake angle of 20° and the tool “B” has a rake angle of 0°. The tool geometries were tested for both materials in the study under orthogonal machining configuration.

#### 4.2.3 Cutting Parameters

To determine the lubrication influence on the tool wear when machining titanium alloys, experimental tests were performed with and without lubrication. These investigations are added to the analysis of the influence of the material microstructure, tool geometry and coating on machinability titanium alloys. However, machining is a manufacturing process with a large number of interacting variables. The produced geometry is influenced by many variables, such as cutting speed, feed, depth of cut, etc. Therefore, the cutting conditions of Table 4.4 are taken into account to achieve a parametric study on orthogonal cutting.

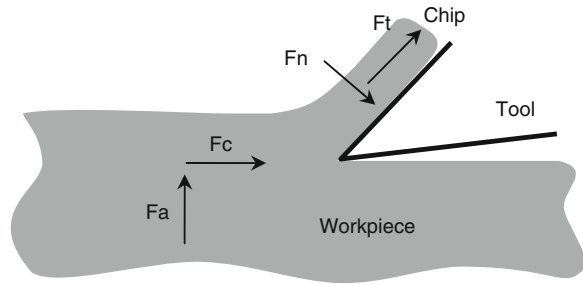
Thus, all these parameters (cutting conditions, tool coating and geometry and lubrication) were considered as wear factors in this work to investigate the influence of cutting forces, friction coefficient, cutting temperature, chip formation process on tool wear.

As shown by Table 4.4, experiments were carried out keeping cutting speed and rake angle at various levels. The range of each factor was selected based on the present day industrial requirements. The cutting length allowed by the machine

**Table 4.4** Cutting conditions and tool geometry

Cutting speed $V_c$ (m/min)	20	35	65
Feed $f$ (mm/rev)	0, 1	0, 1	0, 1
Rake angle ( $^\circ$ )	0 and $20^\circ$	0 and $20^\circ$	0 and $20^\circ$
Flank angle ( $^\circ$ )	$7^\circ$	$7^\circ$	$7^\circ$

**Fig. 4.4** Cutting forces and their direction in the machining plane. ( $F_c$ : Cutting force,  $F_a$ : Feed force,  $F_t$ : Tangential force,  $F_n$ : Normal force)



capacity (about 1.5 m) provides a sufficient cutting time to reach a stationary regime of the cutting process (1.6 s for a cutting speed of 65 m/min).

All experiments were carried out with a constant width of 3.5 mm. The other variables such as machine condition, variability in set up, etc. have been maintained constant throughout the experimentation. A three component Kistler<sup>®</sup> dynamometer was employed for cutting force measurements (Fig. 4.4). The forces reported are those for the process in a stable state with almost steady pulses.

## 4.2.4 Thermal Characterization of Titanium Alloys

### 4.2.4.1 Temperature Measurements

The cutting temperature was estimated using two techniques: the first technique is based on measurements with infrared camera (*Cedip camera*); and the second technique is based on an inverse measurement method using thermistor located behind the cutting tool edge. The last technique was previously developed by Battaglia et al. in [22].

Infrared camera provides directly the thermal field which only gives an assessment of temperature levels. This technique allows a qualitative analysis, unfortunately it cannot be used to determine with high precision temperature values on the cutting tool surface. This is due on one hand to the complexity of the instrumentation, and on the other hand to the confinement of the contact area between tool, chip and workpiece. Table 4.5 presents mean values of the cutting temperature in the case of machining Ti-55531. These measurements were performed using two different cutting speeds ( $V = 20$  m/min and  $V = 65$  m/min).



**Table 4.5** Mean temperature obtained by infrared camera technique (Cedip camera) when machining Ti-55531 with WC-6 %Co tool

Cutting speed (m/min)	Temperature (°C)
20	628
65	761

**Table 4.6** Estimated temperatures during machining of Ti-55531 using thermistors

Cutting speed (m/min)	Temperature (°C)
20	450
65	800

In contrast with the first technique, the second method uses thermistors and provides an indirect measurement of the cutting temperature. The thermistor (very small thermocouple with diameter  $d = 470 \mu\text{m}$ ) is placed in a hole made by electroerosion process inside the tool without embrittlement of its integrity. Thermistors are held fixed close to the cutting tool face. This makes possible to obtain measurements of the heat flux transmitted to the cutting tool. Using the inverse model, developed by Battaglia et al. in [22], an average temperature can be obtained with the measured heat flux taken as an input parameter of the model. We recall here that this type of measurement can not be performed in the case of lubricated machining to avoid disturbance of the thermal field.

Table 4.6 shows the average temperatures estimated when machining Ti-55531 with two cutting speeds ( $V = 20 \text{ m/min}$  and  $V = 65 \text{ m/min}$ ).

As a conclusion on the temperature measurements study, it can be said that whatever the used cutting speed, no phase transition should be expected, since the corresponding cutting temperature remains less than the  $\beta$  transus of titanium alloys which is about  $880 \text{ }^\circ\text{C}$ .

Therefore no phase transition happens in the microstructure, confirming the assumption of Puerta Velasquez et al. in [23]. The later reported that only a severe shearing occurs in the titanium material during machining.

#### 4.2.4.2 Thermal Conductivity Measurements

Before starting the analysis, it very important to remind the evolution of thermal conductivities for the considered titanium alloys with temperature (Fig. 4.5). This has directly an impact on the evolution of tool wear. The data used for plotting Fig. 4.5, were obtained by measuring thermal conductivities using “Hot Disk” method for several specimens under different temperatures [24]. The high temperatures were close to those obtained during machining the same materials.

Ti-55531 and Ti-6Al-4V alloys show a clear difference of about 30 % in their thermal conductivities at  $700 \text{ }^\circ\text{C}$  (Fig. 4.5). At high temperatures, the Ti-55531 alloy conducts heat better than the Ti-6Al-4V alloy. This result is very interesting since it

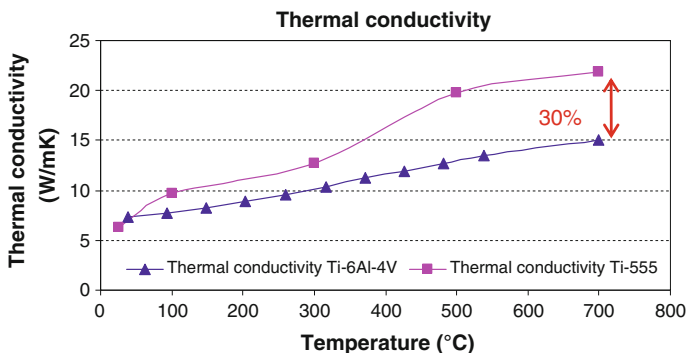


**Fig. 4.5** Evolution of thermal conductivities of Ti-55531 and Ti-6Al-4V with cutting temperature

allows us to explain the morphology observed of formed chips and the variation in cutting forces. Indeed, a low thermal conductivity promotes chip segmentation and thus a reduction of the machining efforts; this is the case for Ti-6Al-4V alloy [25]. When the thermal conductivity increases, the heat stored in the machined material is discharged to the chip and then the ability of the machined material to soften is reduced. Under these conditions, the machining efforts will not fall because of the material flow stress which remains high even at very high temperatures, as in the case for the Ti-55531 alloy. Based on these findings, the degradation modes of the cutting tool could be of a mechanical type for Ti-55531 (abrasion mode) and physico-chemical for Ti-6Al-4V (adhesion and diffusion modes).

#### 4.2.5 Monitoring of the Chip Formation Process

The study of the formation and the nature of chips is one of parameters used to characterize the machining. Due to the fact that machining process is very fast even at low cutting speeds, a high-speed camera (CCD) is used for viewing and monitoring chip formation (Fig. 4.6). The camera used in this study is Phantom<sup>®</sup>. The maximum resolution is  $512 \times 512$ . The acquisition in terms of frames number per second up to 11,000 frames/s. The analysis of different sequences give important information about the physical parameters of machining: worn contact length, deformation level, chips morphology, etc.

### 4.3 Results and Discussion

The obtained results are shown depending on whether one considers the lubricated or dry machining, the use of tools with or without coating. The calculation of the friction coefficient in various cases was also performed. The effects of the tool

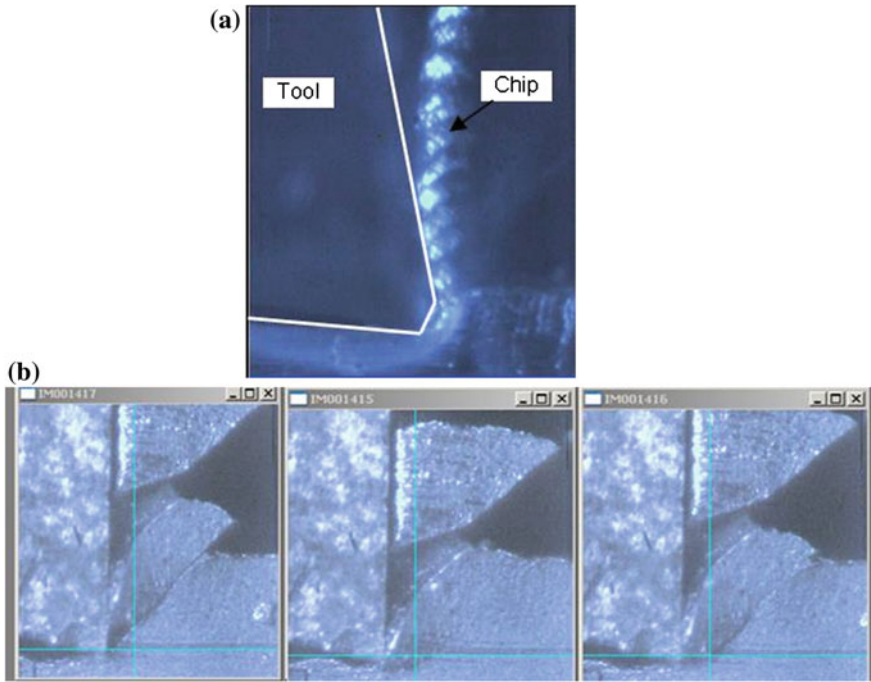


**Fig. 4.6** Chip formation; **a** morphology,  $V_c = 20$  m/min, rake angle =  $0^\circ$ , **b** segmentation process,  $V_c = 65$  m/min, rake angle =  $0^\circ$

geometry and the cutting speed on machinability are analyzed. Also an attempt has been made to examine the effect of various process parameters on the chip morphology and tool wear during machining two different titanium microstructures: Ti-6Al-4V and Ti-55531.

### 4.3.1 Effect of the Tool Geometry

The effect of the tool geometry on the machinability of titanium alloys Ti-6Al-4V and Ti-55531 is presented here with results on both alloys machined with TiAlN coated tools. The analysis of these results has been performed with a comparison on the machinability of the alloys according to the cutting forces, friction and the specific energy of the machining.

#### 4.3.1.1 Effect on Cutting Forces

The cutting forces sign machining quality depending on cutting conditions, tool and workpiece materials. Thus, the measurements of forces give indications on

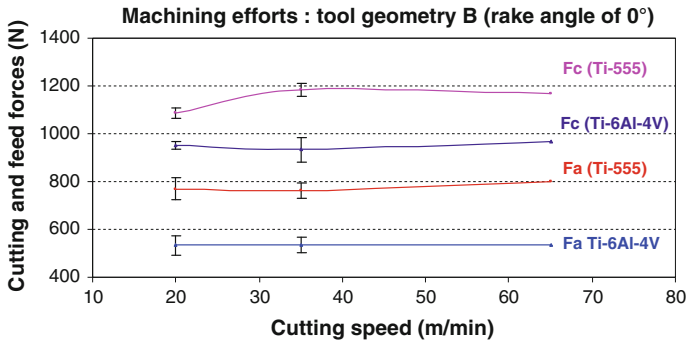


**Fig. 4.7** Cutting forces obtained for Ti-6Al-4V and Ti-55531 with tool geometry “B”

machinability of the machined material. In addition to the friction at the tool/chip interface, cutting forces depend on two main factors: area of the primary and secondary shear planes, and shear strength of the work material at these planes [26].

Figures 4.7 and 4.8 illustrate cutting forces ( $F_c$ ) and feed forces ( $F_a$ ) generated during machining titanium alloys Ti-6Al-4V and Ti-55531. The evolution of machining efforts is plotted as a function of the cutting speed  $V_c$  and the considered tool geometry.

It can be observed from Figs. 4.7 and 4.8 that  $F_c$  is the dominant force component. Therefore, the discussion on cutting forces is focused on the cutting force due the weak variation of feed forces. As seen in Figs. 4.7 and 4.8, the feed force remains stable for all conditions.

First of all, it can be noted from Fig. 4.7, a stabilization of cutting forces with high cutting speeds (35 m/min and 65 m/min). However, a slight increase is still noticeable on the cutting force of the Ti-55531 alloy when cutting speed increases from 20 to 65 m/min. During machining the Ti-6Al-4V alloy with a tool rake angle of  $20^\circ$  (tool geometry “A”) (Fig. 4.8), a reduction of cutting forces is noticed when the cutting speed increases. This is quite normal considering the thermal softening of the material due to the temperature rise during machining. In other words, when the cutting speed increases, the temperature increases too and this is followed by a decrease in the yield stress level of the alloy. The material deforms under these conditions much more easily and without significant effort. This trend is expected because machining becomes more adiabatic and the heat generated in the shear zone can not be conducted away during the very short interval of time during which the material passes through this zone. So, the temperature rise softens the material aiding grain boundary dislocation and thus reducing cutting forces as seen from Fig. 4.8.

However, the cutting speed can not be increased significantly pretext to further reduce the effort because of the significant increase (simultaneously) of the tool wear. On the other hand, an increase in the cutting force level of Ti-55531 with  $20^\circ$  tool rake angle can be observed when increasing the cutting speed. This tendency can be explained by the high strain rate sensitivity of the Ti-55531 alloy.

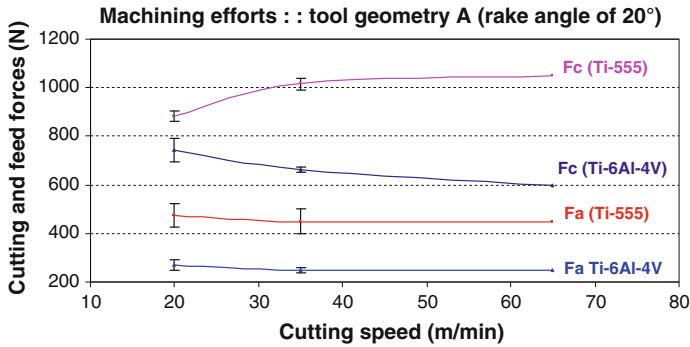


**Fig. 4.8** Cutting forces obtained for Ti-6Al-4V and Ti-55531 with tool geometry “A”

According to Fig. 4.7 the comparison between generated cutting forces shows a clear difference between Ti-6Al-4V and Ti-55531. This difference is ranged from 12.3 to 21.1 % for the cutting force and from 30.1 to 33.4 % for the feed force. This result confirms the poor machinability (previously announced) of the Ti-55531 alloy compared to that of the Ti-6Al-4V under the same machining conditions. The trend given by tools with a rake angle of  $0^\circ$  is confirmed by tools with a rake angle of  $20^\circ$ . The difference may reach 42.9 % for some cutting conditions ( $V = 65$  m/min and  $\alpha = 20^\circ$ ) (see Fig. 4.8).

Also, it was found from Figs. 4.7 and 4.8 that the cutting force obtained with the rake angle of  $20^\circ$  was weak compared to that of machining with  $0^\circ$  rake angle at all levels of considered parameters. This has been attributed to the fact that high values of the rake angle may reduce the friction along the cutting edge between tool and workpiece; see the evolution of the friction coefficient in Sect. 4.3.1.2).

#### 4.3.1.2 Effect on Friction at the Tool/Chip Interface

In this section we focus on the friction, which is the manifestation of the mechanical energy dissipated in the contact between the tool and the workpiece in the form of heat which is responsible for the heating of the cutting edges.

Consequently, to understand physical phenomena during the chip formation, friction process have to be investigated at the tool-chip interface. The friction coefficient is an important parameter to characterize the nature of the tool-chip contact and tool wear depending on cutting conditions. According to the famous model of Merchant [16, 27], the calculation of this parameter can be obtained using cutting forces measurements. In machining, the apparent friction coefficient (or average friction) is often defined as the ratio between the tangential force  $F_t$  and the normal force  $F_n$  [16, 27].

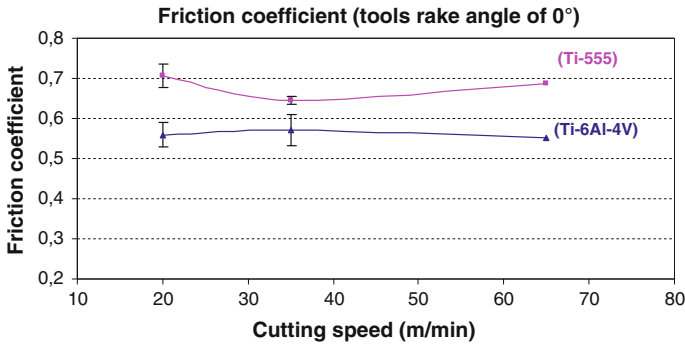


**Fig. 4.9** Evolution of the friction coefficient in the tool/chip interface (Tool geometry “B”, rake angle 0°)

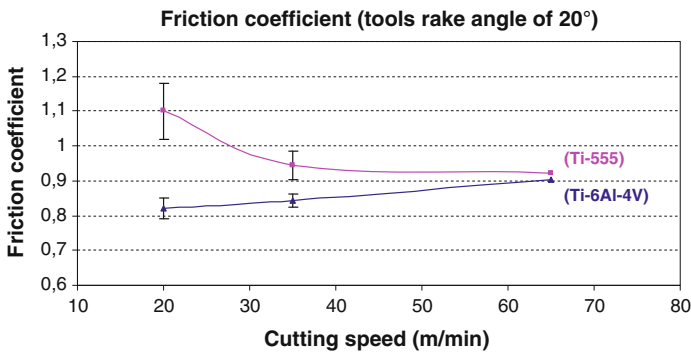


**Fig. 4.10** Evolution of the friction coefficient in the tool/chip interface (Tool geometry “A”, rake angle 20°)

$$\mu = \frac{F_t}{F_n} = \frac{F_a + F_c \tan \alpha}{F_c - F_a \tan \alpha} \tag{4.1}$$

where  $\alpha$  is the rake angle,  $F_c$ : cutting force,  $F_a$ : feed force,  $F_t$ : friction force,  $F_n$ : normal force.

Figures 4.9 and 4.10 show the variation of friction coefficient values at various cutting conditions. These values are calculated using Eq. (4.1). The results of this study show that friction depends on the materials, the cutting temperature and machining conditions (cutting speed, tool geometry, etc.). In all tests, this parameter is more important with tool geometry “A” (rake angle 20°) compared to those with 0° rake angle (tool geometry “B”). This is due to the reduction of the cutting temperature and contact length. This reduction is often followed by a reduction in frictional forces at the tool-workpiece interface. Low cutting temperatures reduce adhesion tendency of the cutting tool and promote contact area restriction. Reduction of the tool–chip contact length is expected to occur,

promotion of the plastic flow at the backside of the chip and overall reduction of temperature.

The results presented above (in Figs. 4.9 and 4.10) show a higher friction coefficient for Ti-55531 compared to Ti-6Al-4V. Thus, the following assumptions can be presented: the contact area at the tool-chip interface can be considered as a sticking contact-type for Ti-55531 in the case of machining with tools of 0° rake angle. Therefore, a connection can be made between the nature of the contact (sticking) and the tendency of Ti-55531 to adhere to the cutting face of the tool. In contrast, the tool-chip contact can be of a sliding type in the case of Ti-6Al-4V because of the low values of friction (see Fig. 4.9). In the case of machining with tools of 20° rake angle (Fig. 4.10), the reduction in friction coefficient for the Ti-55531 indicate contact of sliding type more then sticking one. Contrary to this trend, increasing friction for the Ti-6Al-4V alloy indicate sticking contact. Also, the increase of the cutting speed (in particular for testing tool geometry 20°) involves the stabilization of the friction at high cutting speeds (the friction is a decreasing function of the temperature when the cutting speed increases).

In conclusion, at constant cutting speed, titanium alloy Ti-55531 is more sensitive to adhesion phenomena as Ti-6Al-4V alloy. This may also explain the poor machinability noticed on this alloy.

#### 4.3.1.3 Effect on the Specific Energy in Machining

The specific energy in machining is also a good indicator of machinability of materials. It is calculated based on the cutting conditions and measured forces (Eq. 4.2).

$$u(J/m^3) = \frac{P}{Q} \quad (4.2)$$

with:

$$P = F_c \times V_c \quad (4.3)$$

where  $P$  is the cutting power and  $Q$  is the volume of removed material.

Figures 4.11 and 4.12 confirm the previous analysis of the difference between the machinability of Ti-6Al-4V and Ti-55531. The specific cutting energy is higher for the titanium alloy Ti-55531 to that of Ti-6Al-4V alloy.

It is also interesting to note here the effect of the tool geometry on the materials machinability. With a rake angle of 0° (tool “B”), the difference is around 12 % and remains constant regardless of the cutting speed. With a rake angle of 20° (tool “A”), the difference is greater and reaches high levels for the high cutting speeds [around 51 % for  $V_c = 60$  m/min]

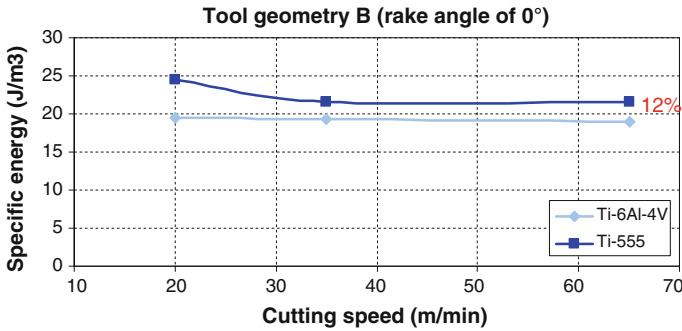


Fig. 4.11 Specific cutting energy for Ti-6Al-4V and Ti-55531, tool geometry “B”

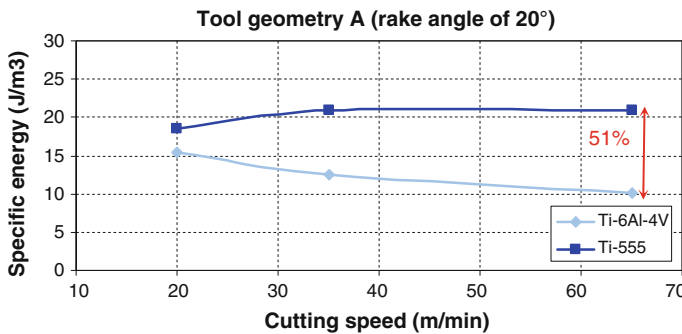


Fig. 4.12 Specific cutting energy for Ti-6Al-4V and Ti-55531, tool geometry “A”

### 4.3.2 Effect of Coating on Machinability

Additional tests were conducted on the Ti-55531 alloy to examine the effect of the coating tools on machinability. This is achieved without lubrication to prevent coupling problems. Only the tool geometry “B” with a rake angle of 0° was used. Thereby the tests are carried out under dry machining configuration with uncoated and coated tools with a single layer of TiAlN with average thickness of 4 μm.

Figures 4.13, 4.14 and 4.15 present the evolution of the machining efforts and friction at the tool/chip interface according to two cutting speeds 20 and 65 m/min.

It can be noted that for the same cutting conditions, the cutting forces obtained with the coated tool when machining Ti-55531 alloy are smaller than those obtained with the uncoated tools. The difference between the two cases is about 8 % for a cutting speed of 20 m/min. This difference is further increased when the speed increases, it reaches 24 % for 65 m/min. This shows that the coating improves significantly the machinability of the material. We can also observe from these results that the coated tools allow a reduction of efforts when the cutting speed increases for Ti-55531 alloy. The difference between the coated and



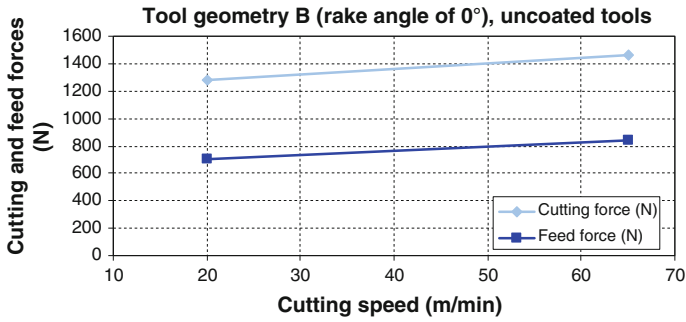


Fig. 4.13 Forces obtained for the Ti-55531 with tool geometry 0°, uncoated tool

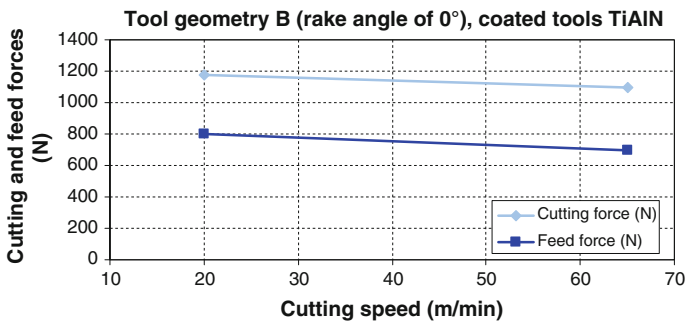


Fig. 4.14 Forces obtained for the Ti-55531 with tool geometry 0°, coated tool

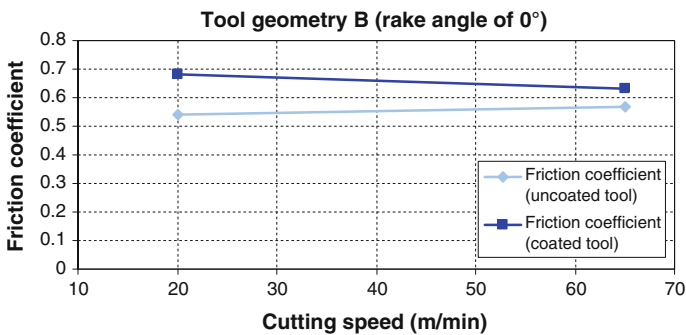
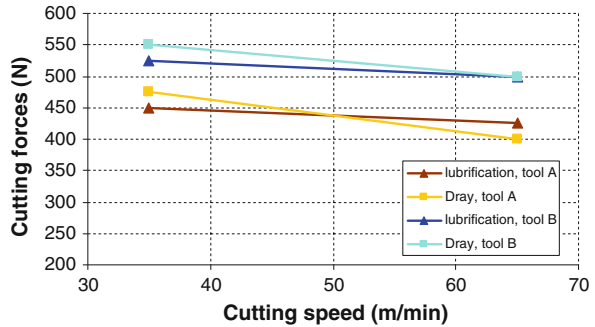


Fig. 4.15 Evolution of the friction coefficient in the tool/chip interface

uncoated tools is explained by the fact that the coating layer, taking into account the thermal and physicochemical characteristics amply improves the tool/chip contact. Its role as a thermal barrier allows the tool to protect themselves against the frictional heating and workpiece to soften more and to deform more easily.

**Fig. 4.16** Machining of Ti-55531 alloy with and without lubrication



This interpretation can be confirmed by the analysis of friction at the tool/chip interface. Coated tools generated an intense friction (sticky type,  $\mu$  close to 1). This means a more intimate contact between the tool and the workpiece. So, heat dissipation into the chips easier. However, the consequence of this contact is the ability to more easily form the bonding layers on the tool surface.

In the case of uncoated tools, friction is lower (0.55–0.57). Such a friction-type promotes a sliding contact and abrasive wear of the tool cutting face. The sliding contact does not facilitate the transmission of heat between the material and the tool, thus the alloy softening becomes difficult. This explains the increase in efforts to form a chip by an uncoated tool relative to a coated tool.

In conclusion, the coating significantly affects the machinability of Ti-55531 by the decrease of the machining efforts and the protection of the tool cutting edge.

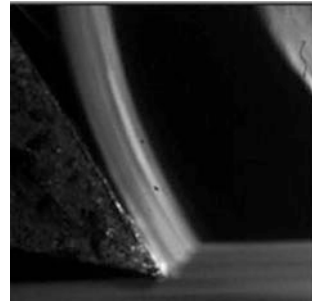
### 4.3.3 Effect of Lubrication on Machinability

To study the effect of the lubrication, several tests were carried. The test results are presented on Fig. 4.16. The data on the Ti-55531 alloy does not clearly show the influence of the lubrication on the cutting forces and hence machinability. However, it has a major effect on tool wear (coated or not). Thus, the analysis shows that lubrication does not directly affect the machinability of Ti-55531 but indirectly via the tool wear. This conclusion differs from the effect of the tool coating; it has a direct effect on machinability and indirect effect on wear.

### 4.3.4 Review of Chips

In this section we present the results of analyzes performed on the chips. Two types of analysis can be discussed here: a microstructural analysis of chips and monitoring their formation with a high-speed camera (CCD).

**Fig. 4.17** Chip formation during machining



#### 4.3.4.1 Chip Morphology of Titanium Alloys Ti-6Al-4V and Ti-55531

During machining and under the action of the tool cutting edge, the workpiece material undergoes a strong compression and deforms plastically. An intense shear is generated between the tool tip engaged in the material and the workpiece (Fig. 4.17). We have analyzed in our investigations this area, called “primary shear zone”, in which occurs the first shear and induces the chip formation.

The chip morphology gives crucial information because it incorporates the material response during machining (mechanical, thermal, thermo-viscoplastic, etc.) and shows the stability of the cutting operation. Moreover, the evolution of cutting forces shows a correlation with the morphology of produced chips. The chip segmentation for example, often leads to a reduction of cutting efforts and the tool-chip contact length. In general, the continuous chip is undesirable in industrial applications. This is due to the generated problems and which significantly affect the machining conditions: damage of the cutting edge, congestion of the cutting area, etc.

The images obtained by the high speed camera (Fig. 4.18a) during machining of Ti-6Al-4V show a segmented chip. To confirm this observation further investigation were carried out on chips collected after machining. The micrographs obtained on these chips show a fairly regular segmentation (Fig. 4.18b). Between two consecutive segments of a single chip, the plastic deformation is very intense and localized in a thin zone of a few micrometers (Fig. 4.19). This area where the plastic deformation is localized is known as adiabatic shear band; it is the seat of extreme shear. The thickness of the shear band was measured for different cutting conditions and its evolution was followed depending on the material nature and on the value of cutting speed. The conclusion of this analysis is that the increase of cutting speed means that the shear bands are more refined in the chip body (Fig. 4.19).

Unlike Ti-6Al-4V, Ti-55531 chips have a morphology slightly scalloped with a rather continuous nature. They are also characterized by highly irregular thicknesses. This morphology retains the same characteristics at different cutting speeds and for the different geometries tested (Fig. 4.20).

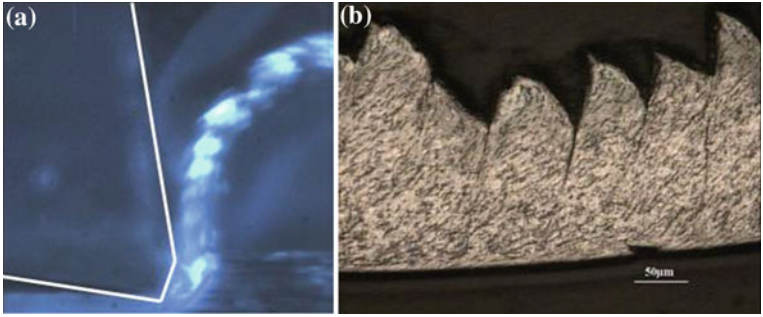


**Fig. 4.18** Ti-6Al-4V alloy chip. **a** Chip formation (Ti-6Al-4V, 20 m/min, rake angle 0° (by high speed camera), **b** Chip morphology (Ti-6Al-4V, 35 m/min, rake angle 0°)

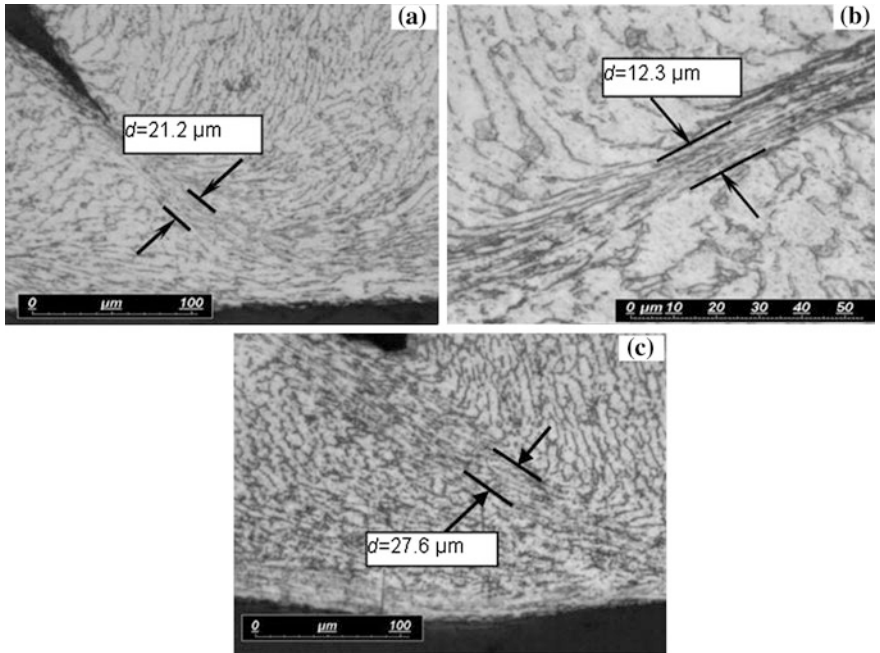


**Fig. 4.19** Evolution of the adiabatic shear band thickness depending on the cutting speed for the Ti-6Al-4V. **a** 20 m/min, **b** 35 m/min, **c** 65 m/min. Tests without lubrication

Figure 4.21 shows the appearance of pronounced adiabatic shear bands without cracking or separation between the chip segments. So, the segmentation being synonyms of lower cutting efforts, during machining Ti-55531 alloy cutting efforts will not decrease even if cutting speed increases. This explains the poor machinability of Ti-55531 compared to the Ti-6Al-4V alloy.

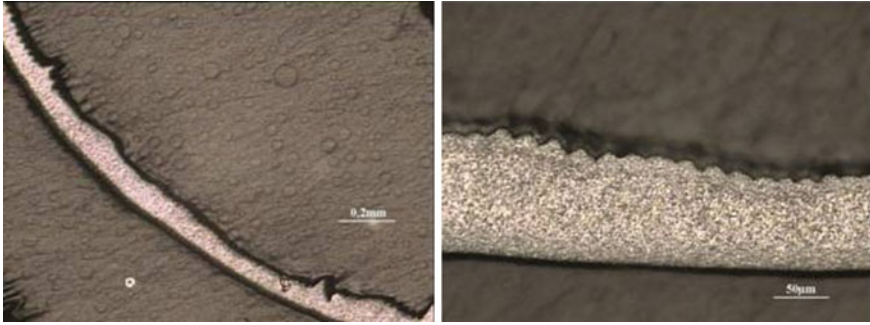


**Fig. 4.20** Chip morphology of Ti-55531 (15 m/min, tool A)

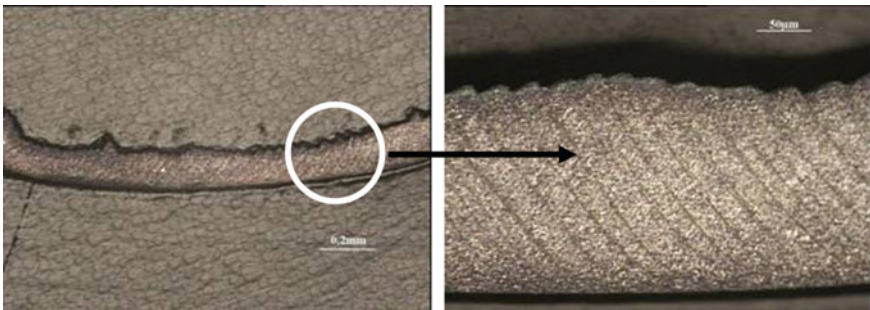


**Fig. 4.21** Chip morphology of Ti-55531 (30 m/min, tool A)

Finally, under the same machining conditions and tool geometries, it can be seen that Ti-6Al-4V forms segmented chips more easily than the Ti-55531. This segmentation allows improved machinability resulted in lower cutting forces.

#### 4.3.4.2 Chip Microstructure of Titanium Alloys Ti-6Al-4V and Ti-55531

Chips obtained after machining and presented in Fig. 4.22 were mounted with epoxy so that they stood on their edge in order to make the cross-section after polishing straight across its length. The polished chips and as-received workpiece material were etched with Kroll's reagent to reveal their microstructures. Micrographs of examined chips in Fig. 4.22 show clearly the deformation phenomenon inside the microstructure of both materials during the chip formation. However, the deformation process is different from one material to the other. It can be noted here that both chips given by machining Ti-6Al-4V and Ti-55531 alloys were obtained with the same cutting conditions.

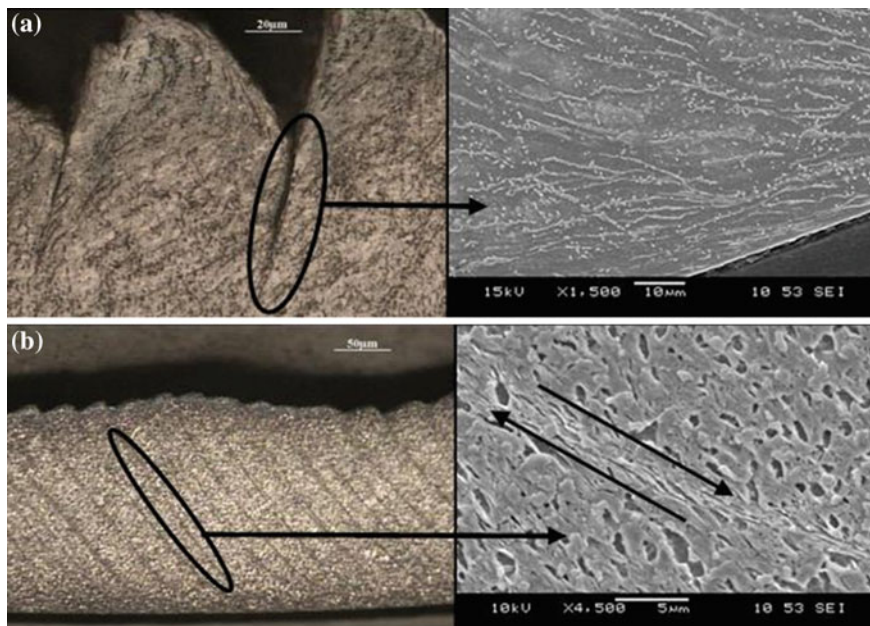


**Fig. 4.22** Microstructure of the chip material obtained after machining. **a** Chip formation and high deformation of  $\beta$  phase for Ti-6Al-4V. **b** Chip formation and very localized deformation of  $\beta$  phase for Ti-55531

The examination of the deformed microstructure reveals very fine sizes of grains in the  $\beta$  alloy (Ti-55531). In this material, the deformation process is localized in a very thin layer called primary shear zone while in the Ti-6Al-4V alloy the same process of deformation occurs in the whole microstructure, i.e. in  $\alpha$ ,  $\beta$  and  $\alpha + \beta$  phases. Indeed, chips of the Ti-6Al-4V alloy have a very different microstructure compared to the initial Ti-6Al-4V alloy. For Ti-55531 chips, apart from the primary shear zone, there is a very similar microstructure to that observed in the initial Ti-55531 alloy.

### 4.3.5 Wear Mechanisms of Cutting Tools

In this section the different modes of tools degradation have been analysed when machining titanium alloys Ti-6Al-4V and Ti-55531. Wear can be discussed in relation to the nature of the material involved, its metallurgical and thermophysical characteristics, machining conditions and the tool coating. The wear analysis is based on observations of the scanning electron microscope (SEM) equipped with energy X-ray spectrometer (EDS) in correlation with the measurements obtained



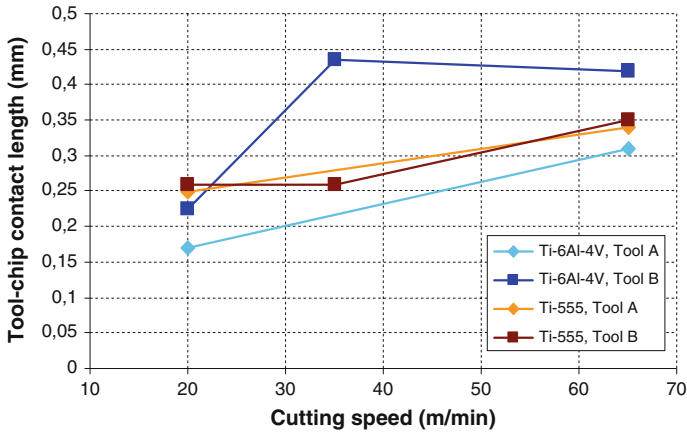


Fig. 4.23 Evolution of the tool-chip worn contact length

with an optical profilometer. The damage modes of tools characterization was conducted through the measurement of:

- The worn tool-chip contact length,
- The thickness and extent of the formed adhesion layers,
- The depth and width of the crater formed on the tool rake face.

#### 4.3.5.1 Study of the Worn Tool-Chip Contact Length

The determination of the worn contact length was performed by analyzing the SEM micrographs of tool-chip contact zones. These areas have previously been identified by measuring the distance between the cutting edge and the limit of the worn portion on the interface. Furthermore, in situ analysis (using a high speed camera CCD) has shown that the chip winding is forwardly of the tool. Thus, the footprint of the wear on the tool surface represents the contact between the latter and the chip being formed. Figure 4.23 summarizes the different values of the recorded worn contact length.

The results show that the increase of the cutting speed induces an increase of the worn contact length. In the case of Ti-6Al-4V the variation is more remarkable. For both tested geometries, it is around 45 %. This confirms the analysis of the heat-softening behavior of material. Indeed, and as mentioned above, the Ti-6Al-4V has a lower thermal conductivity compared to Ti-55531 to the high temperatures (around 30 %). The stored heat thus generates greater softening for the Ti-6Al-4V than for the Ti-55531. The contact between the tool and the Ti-6Al-4V alloy then extends over a larger area of the tool surface relative to the Ti-55531 alloy. For the Ti-55531 alloy, the variation of the contact area is about 25 % when the cutting speed increases from 20 to 65 m/min. The presence of the

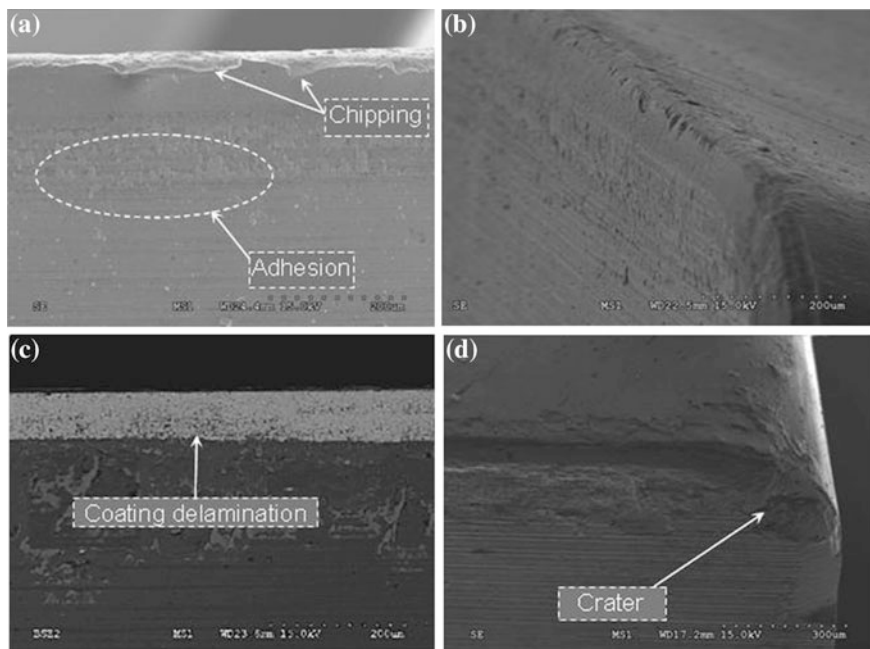


**Fig. 4.24** SEM images (BSE and SE micrographs) of the tool wear when machining Ti-6Al-4V and Ti-55531 alloys with different cutting speeds (rake angle  $0^\circ$ ). **a** SE micrograph (secondary electrons) for cutting tool (machining Ti-6Al-4V),  $V_c = 20$  m/min. **b** SE micrograph (secondary electrons) for cutting tool (machining Ti-55531),  $V_c = 20$  m/min. **c** BSE micrograph (Backscattered electrons) for cutting tool (machining Ti-6Al-4V),  $V_c = 65$  m/min. **d** SE micrograph (secondary electrons) for cutting tool (machining Ti-55531),  $V_c = 65$  m/min

betagenic element chromium in the Ti-55531 microstructure improves the deformation resistance of this alloy at high temperatures. Therefore, the Ti-55531 machinability is degraded as a function of temperature.

In conclusion, it can be said that the affected area by wear in the case of Ti-55531 is greater than in the case of Ti-6Al-4V at identical cutting conditions and tool geometry.

#### 4.3.5.2 Tool Wear Analyses

It has been observed from the SEM analysis in Figs. 4.24 and 4.25 that the cutting tool encounters severe thermal and mechanical loading when machining titanium alloys. This can be supported by the level of the measured cutting temperature (about  $750\text{--}800^\circ\text{C}$  for  $V = 65$  m/min) and high recorded cutting forces (about 1,000 N). Also, other works previously showed that the cutting pressure can also attain large values (about  $1\text{--}1.5$  GPa) [10, 28]. The high stresses and high



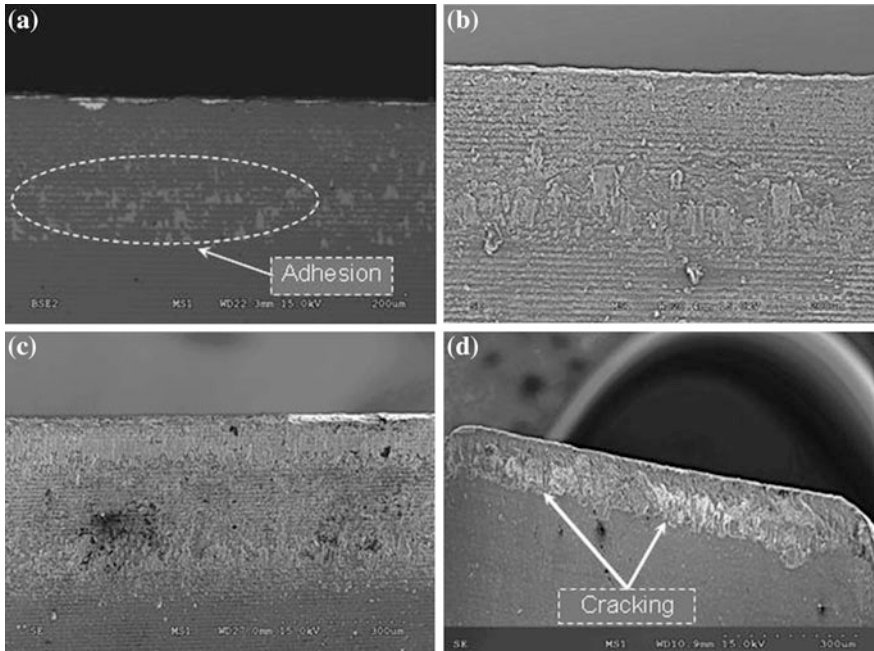


**Fig. 4.25** SEM images of the tool wear when machining Ti-6Al-4V and Ti-55531 alloys (rake angle 20°). **a** Cutting tool (machining Ti-6Al-4V),  $V_c = 20$  m/min. **b** Cutting tool (machining Ti-55531),  $V_c = 20$  m/min. **c** Cutting tool (machining Ti-6Al-4V),  $V_c = 65$  m/min. **d** Cutting tool (machining Ti-55531),  $V_c = 65$  m/min

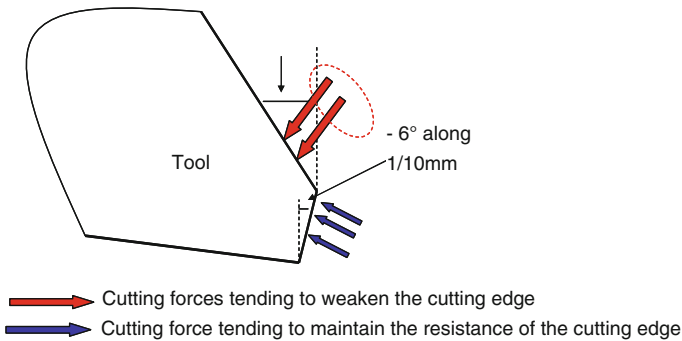


**Fig. 4.26** Orientation of machining efforts on a tool edge

temperatures generated close to the cutting edge have great influence on the tool wear rate and on tool life.

The tool geometry “B” has been designed primarily to give a negative rake angle to the front of the cutting edge (about 0.1 mm). This allows steering the cutting forces inwardly of the tool (Fig. 4.26). The aim of this treatment undergone

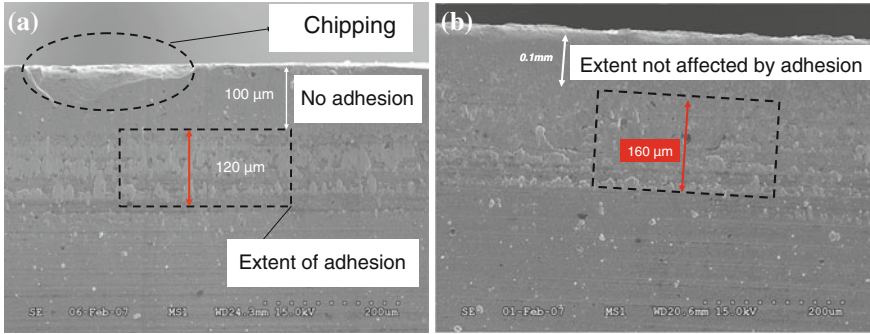


**Fig. 4.27** Adhesion extent on tool geometry B ( $V_c = 15$  m/min), **a** Ti-6Al-4V, **b** Ti-55531

by the cutting edge is to enhance the tool wear resistance. However, the test results showed a significant deterioration of machinability in terms of cutting forces compared to the tool geometry “A”.

From Fig. 4.27, at identical machining conditions, it can be noted that the extent of the negative rake angle of 0.1 mm is not degraded by the adhesion process but only by abrasion wear. The most tangible explanation to this observation is that this area of the tool displaces (or rejects) the material rather than machined.

In the case of tools with  $0^\circ$  rake angle, the extent of the area affected by the wear is greater for Ti-55531 than for Ti-6Al-4V. At 20 m/min for example, it is about 120 μm for the Ti-6Al-4V while about 160 μm for Ti-55531 (Fig. 4.24a, b). This is mainly due to the fact that the increase in cutting forces for the Ti-55531 generates higher stress on the cutting edge. The hardness of the material also contributes to the heavy wear edge. Micrographs also show delamination of the coating layer on the tool surface during machining Ti-6Al-4V at 65 m/min. This is not the case for the Ti-55531 alloy under the same cutting speed (Fig. 4.24c, d).

The delamination phenomenon is difficult to analyze because it can have both thermal and mechanical origins. This is partly due to the complex interaction between various physical factors that control delamination: intrinsic properties of the coating, tool and those of the interaction between the substrate, coating and workpiece. However, it is possible to attribute the origin of delamination to chemical reactions. During cutting of Ti-6Al-4V, adhesion occurring at the tool-chip interface is the main harbinger of the delamination problem.

At low cutting speeds, adhesive wear mode was observed during machining titanium alloys (Fig. 4.24). The location of the adhesion wear is greater in the case of Ti-6Al-4V compared to Ti-55531. For Ti-55531, the wear results show that the predominant degradation process is abrasion wear (Fig. 4.24b).

As shown by the EDS analysis illustrated in Fig. 4.28, particles debris are deposited on the tool surface during machining Ti-6Al-4V as successive layers when chips scroll to the surface. This leads to the adhesive wear mode. The latter

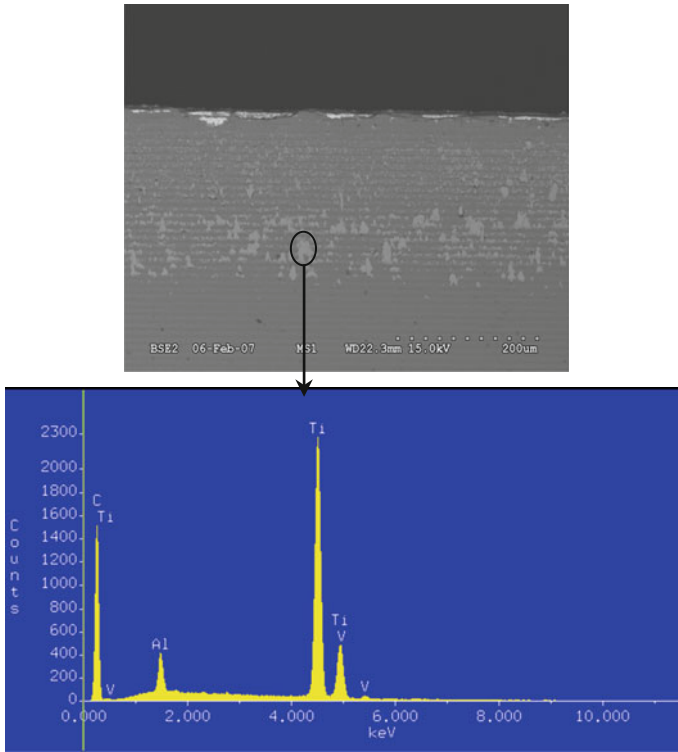


**Fig. 4.28** EDS measurements of the adhered material (Ti-6Al-4V) on the rake face.  $V = 20$  m/min, rake angle  $0^\circ$

is highlighted by the change in the tool geometry and debonding of the coating (Fig. 4.25c).

Auger Electron Spectroscopy (AES) Surface Analysis was also used to verify the occurrence of diffusion process. This technique shows the evolution of the chemical composition at the interface between two different materials. Diffusion profiles were obtained along two lines located in the adhesion zone and inside the worn tool. The AES Surface Analysis performed on the cutting tool (Fig. 4.29a) show along L1 and L2 in Fig. 4.29b, c respectively the evolution of chemical species from the interface between the adhered material on the tool surface till some micrometers inside the tool substrate. It can be clearly showed from this figures that diffusion process occurred between the machined titanium alloys and cutting tool during machining. Diffusion profiles clearly show the diffusion of chemical species from the machined material (Ti, Al, V) to the cutting tool (W, Co, C) and vice versa. This diffusion process can be considered as a process which can generate adhesion wear of the cutting tool and/or delamination of coating.

During machining Ti-55531 at 65 m/min, a process of cracking starts resulting in a collapse of the cutting edge (Figs. 4.24d and 4.25d). This is produced by the

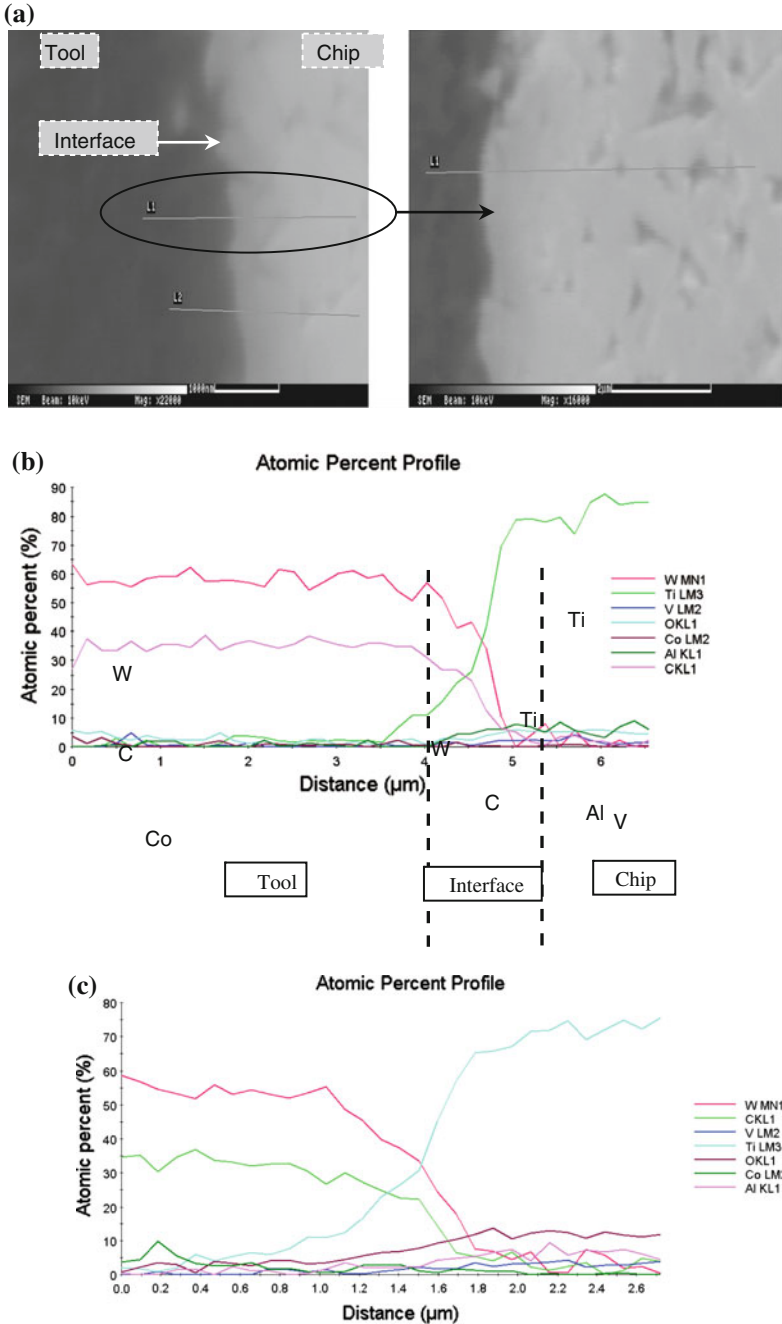


**Fig. 4.29** Diffusion profiles obtained at the tool-chip interface by AES surface analysis along Lines L1 and L2 in the tool-chip interface and inside the cutting tool (Cutting conditions are identical to those of Fig. 4.28). **a** Localization of the analyzed worn zones inside the cutting tool (L1, L2). **b** AES surface analysis along line L1. **c** AES surface analysis along line L2

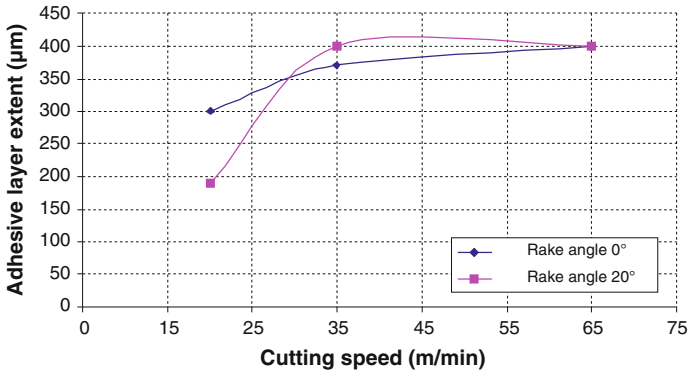


**Fig. 4.30** Evolution of the adhesive layer extent on the tool surface during machining Ti-6Al-4V with different cutting speeds

combined effect of high pressures and large strain rates in the tool (substrate and coating). Adhesive wear layers on the tool surface were measured using a profilometer in the case of machining Ti-6Al-4V. Figure 4.30 shows the evolution of the adhesive layer extent versus cutting speed.

It appears from this result that the adhesive wear increases with the cutting speed and it stabilized at high speeds. This may be due to the diffusion process between titanium alloy and the cutting tool at the interface.

In some cases and under the combined effect of pressure and temperature, welds are formed between tool and chip. With permanent mechanical stress (during machining), these welds are broken thereby causing chipping of the cutting surface. The irregularity on the tool surface can constitute attachment points for chip debris. By accumulating, they eventually form a detrimental macroscopic deposit on the cutting edge. This phenomenon has been observed for cutting tools when machining the Ti-6Al-4V alloy under low cutting speeds (see Figs. 4.24a and 4.25a).

Topographical survey using the profilometer (Fig. 4.31) confirmed that the tool wear exhibited when the machining of the Ti-55531 alloy changes the geometry of the cutting edge. Cracking is due to a fatigue phenomenon of the cutting edge followed by a break of the tool under cyclic loading during machining. The tool with 20° rake angle showed resistance to wear by fatigue and plastic deformation in the case of Ti-55531. Indeed, this geometry improves the flow of chips and material deformation.

In the case of Ti-6Al-4V, the average grain size is about 10 µm and the measured micro-hardness is in the range of 317 HV<sub>0.2</sub>. For the Ti-55531, the microstructure is homogeneous and the grain size is about 1 µm with a micro-hardness of 379 HV<sub>0.2</sub>. From a metallurgical point of view, the major difference between the Ti-6Al-4V and Ti-55531 is due to fineness of the microstructure. This generally leads to a higher mechanical strength. However this will strongly influence the machinability of the machined material and then tool wear as confirmed by Powell and Duggan [29] and by Arrazola et al. in [30]. In addition, the

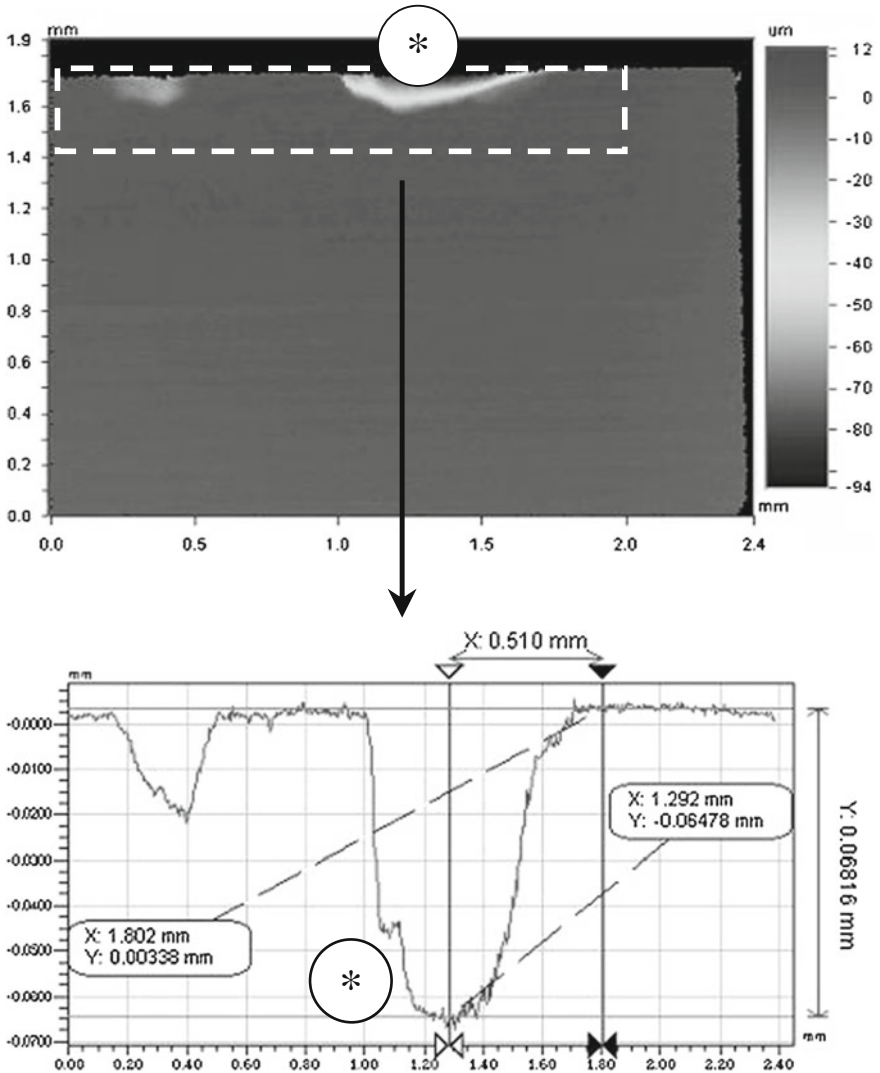


**Fig. 4.31** Worn tool when machining Ti-55531 analyzed by optical profilometer. \*Notched wear with depth of 61  $\mu\text{m}$

Ti-55531 is an alloy of  $\beta$ -type (near- $\beta$  titanium alloy), with the presence of betagenic elements, such as chromium, for example, which limits the ability of the material to deform during machining.

Based on the results from the experimental tests we can give some ideas to improve the machining of the two alloys studied in this article. It is possible to increase the cutting speed in the case of machining Ti-6Al-4V, which causes the increase in temperature at the interface tool/material and therefore a significant

softening of the machined material. Consequently cutting efforts will be lower. This solution can not be applied in the case of Ti-55531 because of its high strain rate sensitivity.

On the other hand, the improvement of the machining of Ti-6Al-4V can be carried out by changing the geometry of the tool. Increasing rake angle facilitates chip flow; this will cause reduction in cutting efforts and pressure. This improvement can also be applied to the machining Ti-55531 alloy.

## 4.4 Conclusion

In this research work, a detailed experimental approach for the comprehension of machining titanium alloys has been presented. Several analyzes (SEM, EDS, AES, Infrared camera, high-speed camera CCD and profilometer analysis) confirmed that differences in machinability and microstructure of tested titanium alloys can have an important impact on tool wear. The low machinability of titanium alloys due to the low thermal conductivity and high microhardness of these materials leads to severe and premature tool wear. The machining of titanium alloy Ti-55531 has been confronted with that of the Ti-6Al-4V alloy. To do this study, the mechanical, thermal, metallurgical and physico-chemical aspects have been deeply analyzed.

During the evolution of the machining efforts depending on cutting conditions and tool geometry, a decrease of cutting forces is noted for the case of Ti-6Al-4V when the cutting speed increases. This decrease is due to the thermal softening of the material under the effect of plastic deformation and cutting temperature. In other words, during the machining of Ti-6Al-4V, its yield stress decreases and therefore improves the machinability for this material. For the Ti-55531, this reduction has not been clearly identified. Unlike the Ti-6Al-4V alloys, the chip morphology of Ti-55531 shows a work hardening behavior. This means that a flow stress increases during machining making more difficult its machinability.

From a metallurgical point of view, the major difference between the Ti-6Al-4V and Ti-55531 is the fineness of the microstructure. The latter is automatically accompanied by a higher strength, better ductility and toughness. It can therefore be said that the Ti-55531 has a better fatigue resistance which greatly penalizes its machinability. Another difference from the Ti-55531 relative to the Ti-6Al-4V is the fact that the microstructure of Ti-55531 contains a volume fraction of the larger  $\beta$  phase. This increases its hardness while also reducing its machinability.

Results have also shown that the friction between the tool and the workpiece is close to 1 for the case of Ti-55531 alloy compared to Ti-6Al-4V. This means that during Ti-55531 machining the contact at the chip-tool interface is of a sticky type, thereby giving trend to the Ti-55531 alloy to more easily adhere to the cutting tool face. This type of contact also influences the thermal field which will be greater in the case of Ti-55531 (temperature for Ti-55531 about 800 °C, for Ti-6Al-4V about 670 °C). In addition, at the high temperatures, Ti-55531 alloy conducts heat better than the Ti-6Al-4V alloy. The low thermal conductivity of the Ti-6Al-4V

promotes chip segmentation and therefore the reduction of machining efforts. For the Ti-55531 alloy, its higher conductivity allows it to further evacuate the stored heat, but at the same time it decreases its ability to soften and thereby deteriorates its machinability. Thus, it is found that the area affected by the wear in the case of Ti-55531 is greater than in the case of Ti-6Al-4V under the same machining conditions and for the same tool geometry.

The rest of our study also showed that the tool geometry has a significant influence on the machinability of both titanium alloys. With a rake angle of  $0^\circ$ , the difference of machinability is only about 12 % between Ti-55531 and Ti-6Al-4V and remains constant regardless of the cutting speed. With geometry of  $20^\circ$ , this difference is greater and reached high levels for high cutting speeds (approximately 34.7–65 m/min).

Regarding the coating, a difference of 8 % (20 m/min cutting speed) was found between the cutting forces when machining Ti-55531 alloy under the same conditions with coated and uncoated tools. This difference further increase as the cutting speed increases, it reaches 24 % for 65 m/min. The coating can therefore significantly improve the machinability of Ti-55531. However, further investigations with different types of coatings are necessary to understand the coating behavior for the optimization of titanium alloys machinability, specifically for the Ti-55531 alloy. The lubrication effect is more marked on the tool damage (with or without coating). Thus, the analysis showed that the lubrication indirectly affects the machinability of titanium alloys through tool wear. This finding differs from the effect of the coating which shows a direct effect on machinability and indirect effect on tool wear.

## References

1. Boyer RR (1996) An overview on the use of titanium in the aerospace industry. *Mater Sci Eng* 213A:103–114
2. Ginting A, Nouari M (2009) Surface integrity of dry machined titanium alloys. *Int J Mach Tools Manuf* 49(3–4):325–332
3. Clément N, Lenain A, Jacques PJ (2007) Mechanical property optimization via microstructural control of new metastable beta Titanium alloys, processing and characterizing Titanium alloys overview. *JOM* 59:50–53
4. Clement N et al (2005) In: JM Howe et al (ed) *Proceedings of international conference solid-solid phase transformations in inorganic materials*. TMS, Warrendale, PA, pp 603–608
5. Nouari M, Ginting A (2006) Wear characteristics and performance of multi-layer CVD-coated alloyed carbide tool in dry end milling of titanium alloy. *Surf Coat Technol* 200(18–19):5663–5676
6. Ginting A, Nouari M (2006) Experimental and numerical studies on the performance of alloyed carbide tool in dry milling of aerospace material. *Int J Mach Tools Manuf* 46(7–8):758–768
7. Nouari M, Makich H (2013) Experimental investigation on the effect of the material microstructure on tool wear when machining hard titanium alloys: Ti-6Al-4V and Ti-555. *Int J Refract Metal Hard Mater* 41:259–269
8. Ginting A, Nouari M (2007) Optimal cutting conditions when dry end milling the aeroengine material Ti-6242S. *J Mater Process Technol* 184:319–324



9. Komanduri R (1981) Turkovich B.F.V., new observations on the mechanism of chip formation when machining titanium alloys. *Wear* 69:179–188
10. Ezugwu EO, Wang ZM (1997) Titanium alloys and their machinability—a review. *J Mater Process Technol* 68:262–274
11. Subramanian SV, Ingle SS, Kay DAR (1993) Design of coatings to minimize tool crater wear. *Surf Coat Tech* 61:293–299
12. Bouchnak TB (2010) Etude du comportement en sollicitations extrêmes et de l'usinabilité d'un nouvel alliage de titane aéronautique, PhD thesis, Ref. 2010-ENAM-0051, Arts et Métiers ParisTech—Centre d'Angers
13. Fanning JC (2005) Properties of TIMETAL 555 (Ti-5Al-5Mo-5 V-3Cr-0.6Fe). *JMEPEG* 14:788–791
14. Nyakana SL, Fanning JC, Boyer RR (2005) *JMEPEG* 14:799–811
15. Semiatin SL (1999) Seetharaman V, Ghosh AK (1999) Plastic flow, microstructure evolution, and defect formation during primary hot working of titanium and titanium aluminide alloys with lamellar colony microstructures. *Philos Trans R Soc A: Mathe Phys Eng Sci* 357(1756): 1487–1512
16. Jackson M, Dashwood R, Christodoulou L, Flower H (2005) The microstructural evolution of near beta alloy Ti-10 V-2Fe-3Al during subtransus forging. *Metall Mater Trans A* 36:1317–1327
17. Benedetti M, Fontanari V (2004) The effect of bi-modal and lamellar microstructures of Ti-6Al-4V on the behaviour of fatigue cracks emanating from edge-notches. *Fatigue Fract Eng Mater Struct* 27:1073–1089
18. Nouari M, Calamaz M, Girot F (2008) Mécanismes d'usure des outils coupants en usinage à sec de l'alliage de titane aéronautique Ti-6Al-4V, C.R. *Mécanique* 336:772–781
19. Devillez A, Schneider F, Dominiak S, Dudzinski D, Larrouquere D (2007) Cutting forces and wear in dry machining of Inconel 718 with coated carbide tools. *Wear* 262(7–8):931–942
20. Singh Gill S, Singh R, Singh H, Singh J (2011) Investigation on wear behaviour of cryogenically treated TiAlN coated tungsten carbide inserts in turning. *Int J Mach Tools Manuf* 51(1):25–33
21. Castanho J, Vieira M (2003) Effect of ductile layers in mechanical behaviour of TiAlN thin coatings. *J Mater Process Technol* 143:352–357
22. Battaglia JL, Coisb O, Puigsegura L, Oustaloupb A (2001) Solving an inverse heat conduction problem using a non-integer identified model. *Int J Heat Mass Transfer* 44:2671–2680
23. Puerta Velasquez JD, Bolle B, Chevrier P, Geandier G, Tidu A (2007) Metallurgical study on chips obtained by high speed machining of a Ti-6 wt%Al-4 wt%V alloy. *Mater Sci Eng A* 452–453, 469–474
24. He Yi (2005) Rapid thermal conductivity measurement with a hot disk sensor: part 1. *Theoret Considerations Thermochim Acta* 436:122–129
25. Abdel-Aal HA, Nouari M, Mansori ELM (2009) Tribo-energetic correlation of tool thermal properties to wear of WC-Co inserts in high speed dry machining of aeronautical grade titanium alloys. *Wear* 266:432–443
26. Merchant E (1945) Mechanics of the metal cutting process II. Plasticity conditions in orthogonal cutting. *J Appl Phys* 16:318–324
27. Merchant E (1945) Mechanics of the metal cutting process I. Orthogonal cutting and a type 2 chip. *J Appl Phys* 16:267–275
28. Komanduri R (1982) Some clarifications on the mechanics of chip formation when machining titanium alloys. *Wear* 76:15–34
29. Powell BE, Duggan TV (1986) Predicting the onset of high cycle fatigue damage: an engineering application for long crack fatigue threshold data. *Int J Fatigue* 8:187–194
30. Arrazola P-J, Garay A, Iriarte L-M, Armendia M, Marya S, Le Maître F (2009) Machinability of titanium alloys (Ti6Al4 V and Ti555.3). *J Mater Process Technol* 209:2223–2230